

GARL: Genetic Algorithm-Augmented Reinforcement Learning to Detect Violations in Marker-Based Autonomous Landing Systems

Linfeng Liang¹, Yao Deng¹, Kye Morton², Valtteri Kallinen², Alice James¹, Avishkar Seth¹, Endowednes Kuantama¹, Subhas Mukhopadhyay¹, Richard Han¹, Xi Zheng^{1,*}

¹School of Computing, Macquarie University, Australia

²Skyy Network, Australia

Abstract—Automated Uncrewed Aerial Vehicle (UAV) landing is crucial for autonomous UAV services such as monitoring, surveying, and package delivery. It involves detecting landing targets, perceiving obstacles, planning collision-free paths, and controlling UAV movements for safe landing. Failures can lead to significant losses, necessitating rigorous simulation-based testing for safety. Traditional offline testing methods, limited to static environments and predefined trajectories, may miss violation cases caused by dynamic objects like people and animals. Conversely, online testing methods require extensive training time, which is impractical with limited budgets. To address these issues, we introduce GARL, a framework combining a genetic algorithm (GA) and reinforcement learning (RL) for efficient generation of diverse and real landing system failures within a practical budget. GARL employs GA for exploring various environment setups offline, reducing the complexity of RL’s online testing in simulating challenging landing scenarios. Our approach outperforms existing methods by up to 18.35% in violation rate and 58% in diversity metric. We validate most discovered violation types with real-world UAV tests, pioneering the integration of offline and online testing strategies for autonomous systems. This method opens new research directions for online testing, with our code and supplementary material available at https://github.com/lfeng0722/drone_testing/.

Index Terms—UAV auto-landing system, Genetic Algorithm, Reinforcement Learning, Search-based testing.

I. INTRODUCTION

Automated UAV landing, such as the routines available in flight controllers like ArduPilot [6], is vital during final flight stages for targeting ground landing spots. With the growth of autonomous UAV services—monitoring, surveying, and delivery [45], [52], [62]—the reliance on non-manually controlled UAVs is increasing. The addition of ground-truth markers can significantly reduce the risk of accidents [7], [34], [44]. Marker-based landing systems are widely used in logistical and industrial UAV applications to ensure reliable landings for large or expensive payloads [3], [54], [55]. Additionally, “drone in a box” solutions, which require precision landings (less than 10 cm) to charging or docking stations, are an emerging sector needing this capability [16], [17], [48]. However, automated marker-based landings carry risks: failed landings due to adverse weather, incorrect marker identification, and collisions

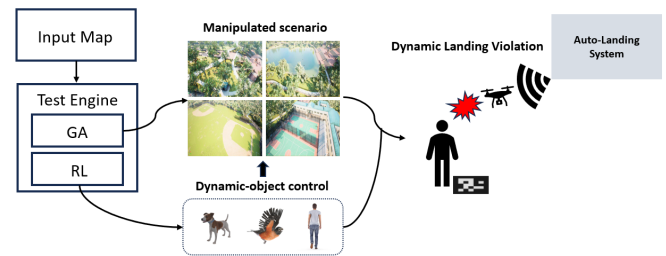


Fig. 1: A high-level overview of GARL framework, including the simulator and the test engine.

with objects. Given stringent safety regulations from authorities like the Federal Aviation Administration (FAA) or European equivalent, and recent incidents, there’s a highlighted need for thorough testing of automated marker-based landings to ensure compliance and safety [2], [12], [13], [63].

Simulation testing is commonly used for Autonomous Driving Systems (ADSs) [15], [25], [37], [39]. UAV operations, including marker-based landings, can similarly be tested using simulation environments like AirSim [51]. Recent studies highlight the potential of offline testing for AI-based cyber-physical systems [59]. However, offline approaches like GA rely on pre-defined configurations for variables such as weather and object positions, limiting their ability to explore the dynamic search space and potentially missing critical corner cases. In contrast, online methods like RL can adjust test cases in real-time but often struggle to converge within limited time due to the extensive learning space in simulation testing [21].

A new method, GA-augmented RL (GARL), is introduced to address the described challenges. Figure 1 depicts a high-level overview of GARL. This approach utilises GA for offline exploration of environmental setup and RL for online management of dynamic object’s movements. As such, GA creates varied environmental conditions in the testing map, while RL manipulates dynamic objects to interact with the auto-landing UAV. This hybrid strategy offers an efficient testing solution, capturing a wide array of violations within

*Corresponding author. Email: james.zheng@mq.edu.au

time constraints, due to the reduction in complexity for RL. Our experiments validate the effectiveness of this integrated approach in overcoming the identified challenges. GARL increases the violation rate by up to 18.35% and increases the diversity of generated violation cases by more than 58% compared to the current state-of-the-art (SOTA) methods. Moreover, most of these additional violation cases have been confirmed as potential violations in real-world settings. Our contributions can be summarised as follows:

- A novel integrated GA-augmented RL (GARL) method to efficiently generate diverse and realistic corner test cases for marker-based UAV landing systems.
- An extensive demonstration of simulation experiments showing that GARL works across different landing systems, increases violation rate by up to 18.35%, and increases the diversity of generated violation cases by more than 58% in comparison to state-of-the-art baselines in various settings.
- A demonstration of equivalent real-world UAV flight tests that validate various simulation-detected violations in recreated practical environments.

II. RELATED WORK

A. GA-based Test Generation

The efficacy of GA has been demonstrated in searching for corner test cases that cause violations and failures in AI-based cyber-physical systems [1], [8], [18], [27], [37], [42], [47], [50]. GA has extensive applications in search-based software testing, and is usually employed as an offline search technique [64]. In [1], [8], the authors proposed new objective functions containing multiple test objectives to guide the search of test scenarios for evaluating Advanced Driver Assistance Systems (ADAS). In [18], a search-based method was proposed to test the pedestrian detection algorithm in Baidu Apollo [4] by manipulating static parameters such as weather and the initial positions of dynamic objects in the test scenarios. AV-FUZZER [37] employs both a global fuzzer and a local fuzzer based on GA to search for corner cases in ADSSs. StellaUAV [50] uses existing GA and different optimisation methods to search for corner cases specifically for obstacle avoidance components. AutoFuzz [68] demonstrates that neural networks have the potential to augment GA and employ a gradient as an indicator to mutate seeds. ScenoRITA [27] proposed new gene representations for testing scenarios to make obstacles fully mutable for finding more meaningful violation scenarios. Recent search-based testing work MOSAT [59] employs GA to manipulate pre-defined driving maneuvers to create diverse violations for ADSSs.

These works focus on new scenario representations, objective functions, and innovative crossover and mutation operations, with test scenarios determined offline. In contrast, we introduce a method that combines a specially designed GA with targeted mutations and crossover operations to enhance the generation of diverse online search spaces for RL. Our approach uses RL to dynamically alter the complex interactions and trajectories

of dynamic objects. This strategy aims to increase violation diversity in marker-based landing scenarios across all components of an automatic landing. In our experiments, we conduct a fair comparison between GARL and a multi-objective GA method, showcasing superior results.

B. RL-based Test Generation

The validity of RL has been demonstrated in generating violation cases in software tests [31], [41]. RL is a Markov Decision Process (MDP) which is built based on an interactive environment that includes agents, actions, policies and rewards [58]. In the MDP, the agent perceives the current state and performs actions in the environment based on the policy to receive the reward. RL agents can serve as offline fuzzers, altering test scenarios based on a reward function, with studies proving their effectiveness in fuzzing [9], [41]. Furthermore, RL can be used for online testing to dynamically create corner cases via a predefined reward function [31], [40]. Research shows that RL-based online testing approaches are able to control dynamic objects in the test scenario in real time to explore more possible violation scenarios [31], [40]. Additionally, D2RL introduces an online RL-based method to fully comprehend the ADS testing environment, despite its high computational demands and long training periods [21].

A common challenge for RL-based methods in simulation testing is the restricted budget, impacting RL agent convergence. A backward training strategy [32] has been proposed to mitigate this by using expert demonstrations in low-fidelity simulations to train the agent before deployment in high-fidelity simulations, which can cause transferability issues. Unlike existing RL-based methods, our framework uniquely combines GA and RL, using GA to simplify RL's learning dimensions. Our surrogate training eliminates the need for expert demonstrations, enhancing agent transferability and allowing direct application in high-fidelity simulations.

C. Combining GA and RL

Combining GA and RL, known as Evolutionary Reinforcement Learning (ERL), has been explored in recent years [29]. ERL utilizes GA to evolve RL policies for addressing path planning and navigation problems [43], [49], [57], [66]. These methods use GA to mutate and evolve RL agent parameters and architectures, focusing on training rather than test generation. Few works combine GA and RL for test generation. For instance, Wuji [67] employs ERL for game testing to find corner cases revealing logical bugs or crashes. In [20], GA and RL are combined to test traditional software, using Q-learning to explore uncovered paths. However, these methods are not directly applicable to autonomous systems with ML modules due to the lack of conventional control structures. To our knowledge, we are the first to combine GA and RL for the test generation of autonomous landing systems.

III. METHOD

A. Overview

The aim of GARL is to generate real and diverse corner cases in marker-based auto-landing scenarios. Figure 2 depicts

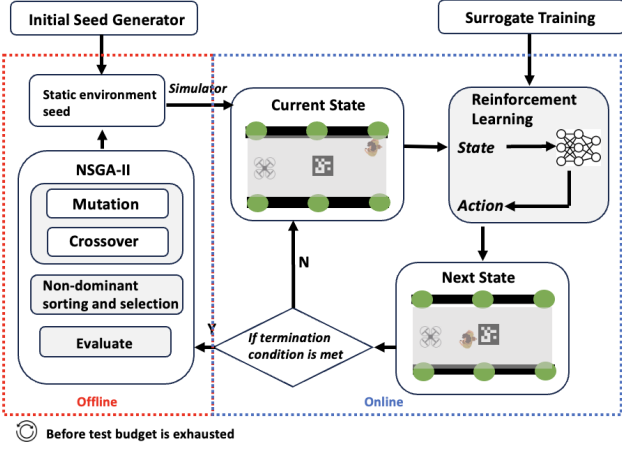


Fig. 2: Workflow of GARN

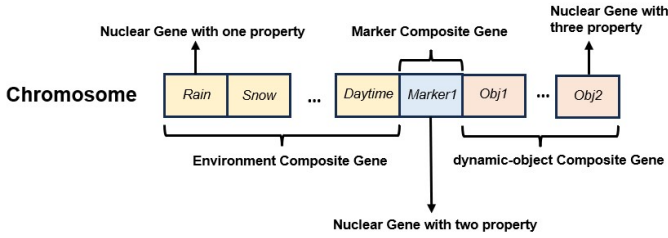


Fig. 3: The Chromosome Representation of Test Case

the workflow of GARN. A seed generator initializes a set of random static environment seeds, each reflecting a specific test scenario. Each seed is input into the simulator, which then allows the RL agent to control NPC objects that interact with the UAV landing process online. Once the termination condition is met, each seed is assigned fitness values for each objective. These seeds are then varied, sorted and selected offline based on the NSGA-II multi-objective GA process to produce new static environment seeds [14]. The workflow terminates when the test budget is exhausted.

B. Modeling Test Scenario

The following factors need to be modelled in the test scenario: UAV landing task, static environment condition, dynamic-object maneuvers. The termination condition is met once the UAV lands or experiences a collision/system crash. The typical workflow of marker-based landing task is defined as follows:

- 1) The UAV is instructed to move to a specified GPS coordinate, referred to as the marker position in this paper, representing the approximate location of the target landing marker.
- 2) The landing system attempts to detect the target marker during the transit flight.
- 3) Once the marker's position is confirmed, the transit flight stops, and the landing begins.
- 4) The landing system controls the landing descent such that the UAV performs a precision landing on the marker.

Figure 3 illustrates our approach, where a static environment is encoded as a chromosome, encapsulating elements like weather, daytime, marker position, and information about available dynamic objects within a test scenario. This chromosome structure includes three composite genes: *environment*, *marker*, and *dynamic object*. The *environment* composite gene comprises single-scalar nuclear genes representing specific environmental conditions, such as *dust*, *fog*, *rain*, *snow*, *road wetness*, *falling maple leaves*, *leaves on the road*, *snow on the road*, and *the sun's position*. These parameters can affect marker detection since we are testing vision-based landing systems. Dust, fog, rain, snow, and falling maple leaves can significantly impact the perception module relying on cameras. Snow and maple leaves on the road can hide the markers, while road wetness can slightly change the color of the ground, affecting detection results. The sun's position affects the time of day and results in different lighting conditions. The *marker* composite gene employs a two-scalar nuclear gene for the (x, y) coordinates of the marker's position. The marker position may cause corner cases, such as being under shadow or glare. The *dynamic-object* composite gene contains multiple three-scalar nuclear genes to define each dynamic object's type, starting point, and velocity. The dynamic objects' position and speed will result in different times to approach the UAV, affecting the online trajectory of the UAV, while the dynamic object's type may affect the detection and sensing result of the auto-landing system. Additionally, the total number of nuclear genes in the *dynamic-object* composite gene matches the variety of object types present in the given scenario. The GA manages this static environment configuration offline. The dynamic-object maneuvers indicate the behaviour of the dynamic object in the simulation. These are dictated by the online RL controls and include moving *up*, *down*, *left*, and *right*.

C. Genetic Algorithm - Offline

In this paper, we present a new genetic algorithm for identifying diverse violation seeds for marker-based UAV landings. Our design features a tailored multi-objective fitness function for our UAV auto-landing scenario, and specialized crossover and mutation operations to enhance seed diversity.

1) Multi-Objective Fitness Function: Our multi-objective fitness function aims to identify varied scenarios that might compromise the safety of UAV landings. Compromises include landing in unmarked zones—areas that might hinder subsequent takeoffs or even lead to crashes. As such, the primary objective addresses incorrect landing positions. Additionally, extended landing durations are also risky due to the significant power consumption of UAVs. An increase in diversity among the population is also critical. Therefore, our multi-objectives can be identified as follows:

- *Distance-To-Landing* (DTL), which measures the deviation from the designated landing marker to assess safety protocol compliance (objective 1).
- *Time-To-Landing* (TTL), which evaluates the required landing duration to identify potential battery-related failures. For instance, the Wingcopter specification sheet indicates

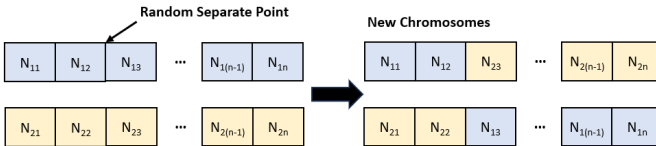


Fig. 4: Process of Nuclear Gene Crossover

that their VTOL is limited to 2 minutes in multi-copter mode, necessitating that landing must occur within that time frame [65] (objective 2).

- *Diversity*, which reflects each seed's uniqueness, calculated by summing the distances between one seed and all other seeds in the generation to ensure a broad range of tested conditions, enhancing reliability. We adopt the novel search diversity calculation (Equation 1) [35], [36].

$$D_i = \frac{1}{k} \sum_{j=1}^k d(x_i, x_j) \quad (1)$$

where D is the diversity metric for each chromosome representation, x_i is the i -th chromosome representation of the test scenario in each generation, x_j is the j -th chromosome representation of the test scenario in each generation, $d(x_i, x_j)$ is a function of calculating Euclidean distance between x_i and x_j , and k is the generation size (objective 3).

2) *Variation Operation*: The *crossover* and *mutation* are used as variation operators. These operators, as indicated in Algorithm 1, are used to manipulate chromosomes after one generation.

Nuclear Gene Crossover: The crossover is a swap operation between two consecutive chromosomes. This aims to swap the nuclear genes between two high-fitness value chromosomes to form new chromosomes that potentially have high fitness values, as indicated in Figure 4. If the crossover rate is met, the process begins by pairing two adjacent selected chromosomes. A random separation point within the chromosome length is chosen. The two paired chromosomes then disconnect from this point and crossover, forming two new chromosomes (line 11 to line 17 in Algorithm 1).

Property-Level Mutation: We design a mutation operation that would increase the diversity among chromosomes. Each property in the nuclear gene undergoes mutation according to the specified mutation rate (line 23 in Algorithm 1) which enhances exploration within the test scenario. Specifically, if the mutation rate is met, m valid candidates for each property are randomly sampled based on the available range (line 25 to 28 in Algorithm 1). Then, the candidate with the maximum distance to that property of all chromosomes in the current generation is set as the value of the property in the current mutated chromosome (line 30 in Algorithm 1).

$$y'_{ij} = m_k, \quad k = \arg \max_{k \in K} \sum_{y \in Y_{ij}} |m_k - y| \quad (2)$$

Algorithm 1 The GA chromosome-based suite of variation operators

```

1: Input: Parents  $P_t$ , Offspring  $O_t$ , crossover threshold  $threshold_c$ , mutation threshold  $threshold_m$ , number of mutation candidates  $m$ 
2: Output:  $P_{t+1}$ ,  $O_{t+1}$ 
3:  $P_{t+1} \leftarrow \emptyset$ ,  $O_{t+1} \leftarrow \emptyset$ 
4:  $R_t \leftarrow P_t \cup O_t$ 
5: for  $i$  in range( $0, |P_t|$ ) do
6:   sort and select parent chromosome  $x_i \in R_t$ 
7:    $P_{t+1} \leftarrow P_{t+1} \cup \{x_i\}$ 
8: end for
9: for each pair of chromosomes  $(x_i, x_j) \in P_{t+1}$  do
10:  generate  $r \sim U(0, 1)$ 
11:  if  $r > threshold_c$  then
12:    generate crossover point  $s \sim U(0, Len(x_i))$ 
13:     $x'_i, x'_j \leftarrow NuclearGeneCrossover(x_i, x_j, s)$ 
14:     $O_{t+1} \leftarrow O_{t+1} \cup \{x'_i, x'_j\}$ 
15:  else
16:     $O_{t+1} \leftarrow O_{t+1} \cup \{x_i, x_j\}$ 
17:  end if
18: end for
19: for each chromosome  $x_i \in O_{t+1}$  do
20:  for each nuclear gene  $y_i \in x_i$  do
21:    for each property  $y_{ij} \in y_i$  do
22:      generate  $r \sim U(0, 1)$ 
23:      if  $r > threshold_m$  then
24:         $M \leftarrow \emptyset$ 
25:        for  $i$  in range( $0, m$ ) do
26:          generate  $c \sim Property Range$ 
27:           $M \leftarrow M \cup \{c\}$ 
28:        end for
29:         $y'_{ij} \leftarrow PropertyMutation(y_{ij}, M)$ 
30:         $y_{ij} = y'_{ij}$ 
31:      end if
32:    end for
33:  end for
34: end for
35: return  $P_{t+1}, O_{t+1}$ 

```

Equation 2 indicates our core mutation strategy, where y'_{ij} is a i -th nuclear gene's j -th property in the chromosome after mutation, K is the total number of mutation candidates, Y_{ij} is a set containing all chromosomes' i -th nuclear gene's j -th property in the current generation.

D. Reinforcement Learning - Online

Within the test scenario, RL guides the dynamic object dynamically in a direction that heightens the probability of violations using a reward function. This is done rather than sampling pre-defined trajectories for the dynamic objects as typically done in GA [59]. Online RL testing faces challenges such as high training variance and long convergence times [21]. To mitigate these, we use a surrogate environment and a

handcrafted reward function for preliminary RL training. The surrogate environment simplifies the learning process, reducing variance and speeding up convergence. Once trained, the agent is directly transferred to the full simulation.

1) Build Surrogate RL Training Environment: The developed surrogate environment is built using the same simulation engine as the full simulation environment. Differently, the surrogate environment features a dynamic object, a marker, and a UAV. In the surrogate environment, the start point of the UAV is generated in the scenario and given the marker's coordinates as a prior. The UAV then flies directly to the marker without any additional trajectory planning. Each training episode begins with the UAV's takeoff and ends with either its landing or a collision. The following restrictions are applied to create a surrogate training environment with lower training variance:

- In the surrogate environment, object animation effects, such as movement, are removed to expedite the process. The training focus is on enabling the RL agent to learn trajectory adjustment based on the UAV and marker positions, making animation effects unnecessary.
- The marker is placed at a fixed point, greatly limiting the agent's exploration and thereby reducing training variance. Since the RL state is described using the relative distances between the marker, UAV, and object, the trained agent remains effective in the full environment.
- In the surrogate environment, a single dynamic object is deployed. After approximately 12 hours of training, the RL agent learns to produce trajectories towards the marker, impacting marker detection and drone landing. We then deploy multiple RL agents in the full environment to control several dynamic objects.

The DQN algorithm is used as it is specifically designed for discrete action spaces [60]. The state (S) of our RL input is a 4-dimensional vector that represents relative positional information between the object, the marker, and the UAV:

$$S = (P_{obj,x} - P_{marker,x}, P_{obj,y} - P_{marker,y}, P_{uav,x} - P_{marker,x}, P_{uav,y} - P_{marker,y}) \quad (3)$$

where P_{obj} and P_{uav} are the positions of the object and the UAV respectively, and P_{marker} is the position of the marker. The definition of the state space is based on the rationale that relative positions more easily transfer between surrogate and full environments.

The dynamic object's action space is discretized into categories of movement. The action space (A) can be denoted as a set that contains 5 actions:

$$A := \{U, D, L, R, S\} \quad (4)$$

where U, D, L, R, S represents moving up, down, left, right, and stationary. The RL agent will choose one action from the whole action space at each time step. As RL makes step-wise decisions at short intervals (0.5 seconds), the accumulated movements form trajectories closely mimic realistic scenarios. Different velocities are set for various object types to closely replicate real-world conditions.

2) Define Reward Function: In the surrogate environment, our dynamic object have two goals: first, to disrupt the UAV's detection of the marker; second, to attempt collision with the UAV. Consequently, a two-part reward function has been designed. Firstly, a semantic segmentation map is collected from the UAV's camera, detailing the marker and the dynamic object, and calculating the percentage of the obstructed area of the marker. Secondly, a collision indicator awards a reward upon collision. The reward function at each time step is defined as follows:

$$\mathbf{R} = \begin{cases} \frac{S_{gt}}{S_d} + \mathbf{I}, & \text{if } S_d \neq 0 \\ \mathbf{I}, & \text{if } S_d = S_{gt} \text{ or } S_d = 0 \end{cases} \quad (5)$$

where S_{gt} is the area of the marker, a ground truth retrieved from the simulator and S_d is the detected area of the marker through the camera at each time step. If $S_{gt} = S_d$, this signifies that the marker is not occupied and results in no reward. Similarly, if $S_d = 0$, it indicates that no marker has been detected which also results in no reward. \mathbf{I} is a collision indicator with a predefined reward value (1 used in our experiments). When a collision happens, the reward will be issued, subsequently concluding the episode. This unique design for surrogate training ensures rapid convergence of the RL agent and efficient transfer between the surrogate and the full environment.

IV. EXPERIMENT

A. Research Questions

The following research questions (RQs) were assessed to evaluate the performance of GARL:

- RQ1: How effectively does the GARL evaluate different marker-based landing systems?
- RQ2: How effective is GARL at exposing landing violations compared to existing state-of-the-art techniques?
- RQ3: Can landing violations found in the simulation be verified in the real world?

B. Experiment Setup

1) Simulation Environment: In experiments, the simulation environment is constructed using AirSim [51], which is an open-source UAV simulation platform based on the Unreal Engine (UE) 4 [19] and widely used in UAV research [33], [53], [56]. AirSim supports rendering high-fidelity scenes and simulating realistic physical and weather effects. Another advantage is that it is flexible to customize and create new simulation maps leveraging resources in UE4. We can also easily extend the ability of AirSim by implementing new APIs to manipulate the simulation environment.

Two maps based on the real-world test fields were chosen by industry research collaborators to construct realistic simulation test environments, as shown in Figure 5. The Court map features a city-like environment with basketball fields, including concrete landing areas, while the Lawn map offers a natural setting. In addition, ArUco markers, a widely deployed type of UAV-landing target, are inserted as UAV landing targets



(a) Court



(b) Lawn

Fig. 5: Example of test map in real-world (First row) and AirSim (Second row).

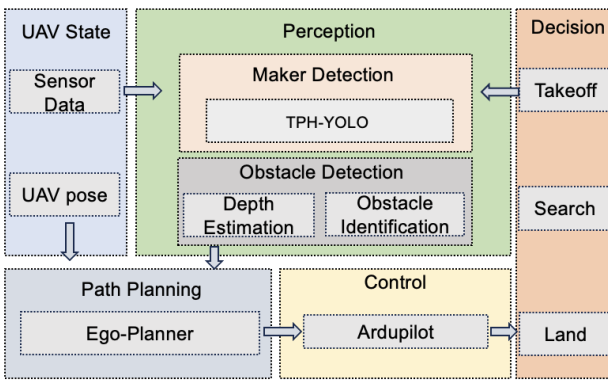


Fig. 6: The system architecture of MM-MLS

("markerID:0"), with an API is provided to place the marker [23], [30]. The selected dynamic object types aim to replicate the variety of dynamics typical in those scenarios, such as aerial movements, low-height ground activities, and interactions involving taller ground elements. Therefore, different types of dynamic objects were added on the ground and in the air of the simulation maps, including persons, birds, and dogs. Corresponding APIs were also implemented to control the dynamic movements. The simulation environments and new APIs can be downloaded from the available software repository (see Abstract).

2) *Marker-based Landing Systems*: Three marker-based landing systems were implemented and integrated into the simulated UAV and tested in the created simulation environments (Table I):

- *OpenCV-MLS*: The system features a perception module utilizing OpenCV [10] for marker detection and position estimation, a decision module to manage the marker-based landing task, and an Airsim-based control module.
- *TPHYolo-MLS*: The architecture mirrors *OpenCV-MLS* but incorporates TPHYolo [70], a deep learning model for marker detection. TPHYolo adopts the transformer mechanism [61] to improve performance when detecting

small-size objects, as proven for use in UAV-related research [70].

- *MM-MLS*: This system is built based on *TPHYolo-MLS*, and introduces ego-planner [69] for trajectory planning. Ego-planner, a leading open-source solution, enables real-time obstacle detection and trajectory planning using depth image data and UAV's pose. The ArduPilot [6] flight control platform directs the UAV to follow the planned trajectory. The detailed system architecture, illustrated in Figure 6.

Though some other marker-based landing systems have been proposed [11], [38], their models were not available as open-source at the time of writing and, thus, were not evaluated in this study.

3) *Implementation Details*: The detailed hyper-parameter setting of our method and the experiment can be found in our supplementary material. Specifically, in simulations, positional parameters are normalized within [-1,1], while weather parameters default to the [0,1] range. To ensure moderate weather conditions, these parameters are confined to [0,0.15].

The number of dynamic objects in the simulation varies with the PC's capabilities. To control for variability due to simulation rendering differences, all experiments are repeated three times using an RTX 3090 GPU, each with a 400-test budget, and average results are reported. The UAV's dimensions are set to one meter in width and length, matching AirSim's default configuration. The target marker is 1.5 meters in width and length, allowing the UAV to land within it if the auto-landing system functions correctly.

C. Experiment Design

1) *RQ1*: We assessed GARN on three landing systems: *OpenCV-MLS*, *TPHYolo-MLS*, and *MM-MLS* in two simulation maps Court and Lawn respectively. Each landing system was assessed by using GARN to generate 400 test scenarios. Data for each scenario run was saved, including the scenario seed, a video recording, the UAV trajectory data, and any UAV-object collision events.

The record was used to identify landing violations of the tested system. A violation occurred if the UAV collided with objects or landed outside the marker's bounds. Given the marker is a 1.5-meter square and the UAV is smaller, a landing position more than 1.5 meters from the marker center ensures it is outside the marker. Considering real-world UAV GPS accuracy is typically within 1-meter [22], we set 1.5 meters as the threshold for landing violations. The *landing violation percentage* was calculated as the ratio of scenarios with violations to the total number of scenarios. This value measures the effectiveness of the GARN method in finding landing violation scenarios.

The saved landing recordings were also analyzed to identify the *violation type*, which qualitatively measures the diversity of violation scenarios that are caused by different reasons. For example, the reason could be false positive marker detection, collision, or even system crashes. The metric *violation type*

TABLE I: The component involved in each SUT

Landing Systems	UAV State	Detection		Planning	Control		Decision
		OpenCV [10]	TPHYolo [70]		Airsim [51]	Ardupilot [6]	
OpenCV-MLS	✓	✓			✓		✓
TPHYolo-MLS	✓			✓	✓		✓
MM-MLS	✓			✓		✓	✓

showcases the GARL’s capability to create a diverse range of landing violation scenarios.

2) *RQ2*: We compared the performance of GARL with five baseline methods on *MM-MLS*, the system currently deployed in the real-world by our industry collaborators, in two simulation maps. The detailed settings of those baselines are listed below:

- 1) *Random*: all the static environments are randomly generated. Additionally, dynamic objects’ start positions and destinations are generated randomly within the specified map range.
- 2) *Multi-Objective GA* [59]: This baseline shares the same fitness function and chromosome representation as GARL, employing NSGA-II [14] to manage these objectives. However, this baseline adds the dynamic object’s destination into the dynamic object composite gene and utilizes a standard mutation strategy. This baseline can also be regarded as an ablation study to indicate the performance of GARL without RL part.
- 3) *Offline RL Fuzzer* [9]: this baseline initiates with a random scenario, and the state encodes the environment, marker position, and dynamic objects’ start and endpoints. The RL agent can alter weather conditions or marker location by ± 0.1 or move a dynamic object’s start or endpoint in one of four directions: up, down, left, or right offline. The reward combines Distance to Landing (DTL), Time to Land (TTL), and diversity to all previously generated scenarios as introduced in Section III-C1. The configuration for the offline RL model, including its exploration strategy (initial epsilon and its decay) and learning rate, parallels our surrogate training protocol. Detailed settings of this baseline can be found in our supplementary material.
- 4) *Online RL* [40]: this baseline allows the RL agent to control weather, daytime, and dynamic objects online. Each simulation starts with a randomly initialized test scenario. The state encodes the environment, marker position, and dynamic objects’ start points. The RL agent can alter the weather by ± 0.01 or move a dynamic object up, down, left, or right. The reward function mirrors that of our surrogate environment. If the action involves moving a dynamic object, a random object will be selected. Detailed settings are provided in our supplementary material.
- 5) *Surrogate trained RL with random*: this baseline serves as an ablation study, replacing the GA offline component in our solution with a random generator.

The efficiency metric is measured as **Top-K** [15], which

evaluates how many test cases are needed to find the first K violation cases. In this paper, the K is set as 10. The *landing violation percentage* metric, used in RQ1, was used to evaluate the percentage of violation in generated test cases. Diversity was measured with two metrics: *parameter distance* and *3-D trajectory coverage*.

Parameter distance was derived from the idea of novel search [35], [36]. A higher parameter distance means the generated violation seeds have a higher diversity. Parameter distance is calculated for all generated test cases as shown in Equation 6:

$$\rho(x) = \frac{1}{n} \sum_{i=1}^n \left[\frac{1}{n} \sum_{j=1}^n d(x_i, x_j) \right] \quad (6)$$

where x_i and x_j are the i -th and j -th test scenario representation vector in all generated scenarios, which contains the environment (weather, daytime), the marker position, and available dynamic object information, $d(x_i, x_j)$ represents the Euclidean distance between x_i and x_j , n is the number of generated test cases.

3D-Trajectory Coverage is a trajectory coverage metric that measures how violated trajectories cover the simulation map, and is adapted from an ADS implementation [26]. We implement the metric in 3D in order to measure the trajectory coverage during a 3D marker-based UAV landing task. The simulation environment is divided into several $2 \times 2 \times 2$ meter cells. A 3-dimensional array is used to index each cell in the grid. All entries in the array are initialized to *false*. An entry’s value is set to *true* if the UAV visits the corresponding grid cell while a violation occurs during that run. The metric calculation is presented as Equation 7:

$$3D - TrajectoryCoverage = \frac{N_{covered}}{N_{total}} \quad (7)$$

where $N_{covered}$ represents the number of grids covered in violation cases, N_{total} denotes total number of cell.

Additionally, we measure the time consumption of each method. While accuracy is crucial, significantly longer test case generation can hinder successful adoption.

3) *RQ3*: Real-world testing was conducted to ensure the generated violation cases were realistic. The *MM-MLS* landing system was implemented on a custom UAV to recreate the simulated errors. This UAV is equipped with a 295mm frame, 5-inch 3-blade propellers, 1750KV motors, an Intel D455 camera, and an NVIDIA Jetson Nano onboard computer. A physical ArUco marker (“markerID:3”) serves as the landing target on the ground. For non-collision violation types, the UAV is programmed to initiate landing after detecting the

TABLE II: Landing violation percentage for different landing systems across two maps

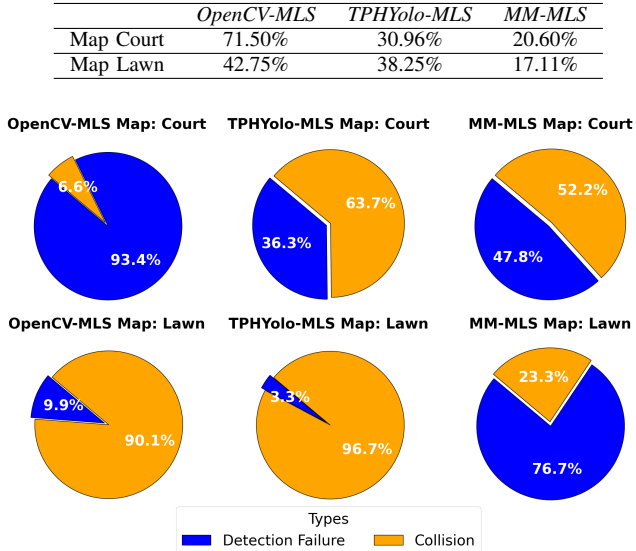


Fig. 7: General violation types found in different systems.

marker continuously for 5 seconds above a 0.7 confidence threshold. For reproducing collision-related violations, we utilize a controlled real-world replication strategy. Specifically, we deployed the auto-landing system on the UAV. The system would output the planned trajectory for landing, but the UAV keeps hovering in the air and does not follow the trajectory to move. The intermediate outputs of the system such as detected obstacles and planned trajectories are recorded and can be visualized in a visualization software called Rviz [28] to check the reaction of the landing system regarding obstacles. By comparing the planned trajectory, we can predict if collisions in simulations would occur under real-world conditions, allowing for a safe assessment of potential collision scenarios without risking actual damage.

V. RESULTS

A. Effectiveness of GARNL across different Auto-Landing systems (RQ1)

Table II showcases the test results of GARNL across three landing systems and different test maps. The results highlight GARNL’s effectiveness in identifying landing violations for these emerging versions of industry-standard UAV landing systems. More advanced versions of landing systems have led to a significant decrease in violations detected, with a notable 40.54% decrease when moving from *OpenCV-MLS* to *TPHYolo-MLS* in the Court map. Furthermore, the transition from *TPHYolo-MLS* to *MM-MLS* saw a further 21.14% decrease in violations detected in the Lawn map.

To compare system performances, we categorized violations into *collision* and *detection failure (of marker)*, shown in Figure 7. The Lawn map, with its uniform green surface, mainly shows collision violations, with minimal interference in marker detection. In contrast, the Court map, featuring

white lines, red areas, and tree roots, presents a greater chance of false positives, thus increasing marker detection failures. Therefore, in the Lawn map, *OpenCV-MLS* and *TPHYolo-MLS* perform similarly without a planning module. However, on the Court map, *OpenCV-MLS* predominantly suffers from *detection failure* due to its less robust detection algorithm, which limits the effect of dynamic objects controlled by GARNL. Conversely, *TPHYolo-MLS* experiences fewer *detection failure* violations, thanks to its superior detection capabilities in detecting smaller objects, enabling more accurate marker identification. Yet, the absence of an obstacle avoidance module under the testing of GARNL significantly raises the risk of dynamic object collisions with the UAV.

We classified the violations observed in simulations into specific categories based on a manual analysis of recorded simulations:

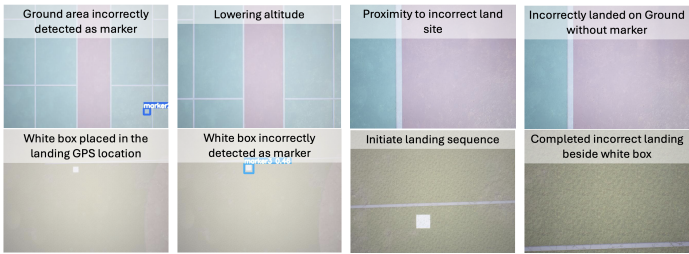
1) *Type I*: The first violation type is incorrect landing due to false positive marker detection. Figure 8a depicts two sequences of landing at incorrect marker locations. The first sequence shows the UAV initiating landing on a ground section erroneously identified as a marker, likely due to ground reflection. Even after losing track of the marker, the UAV proceeds to land incorrectly. The second sequence demonstrates the UAV mistaking a white marker (marker 3 instead of the intended marker 0) as the landing spot and, despite fluctuating confidence, lands there mistakenly.

2) *Type II*: The second type of violation is a failure to land because of a false negative detection. Figure 8b showcases several instances where no marker is detected. In the first provided example, a white static object partially covers the marker, and the day is foggy. These conditions result in the marker not being detected. In the second example, the marker is placed near a bench, and the presence of a nearby black object prevents the marker from being detected. In the third example, the perception module has low confidence in the marker location due to the extreme weather conditions. Consequently, no landing occurs.

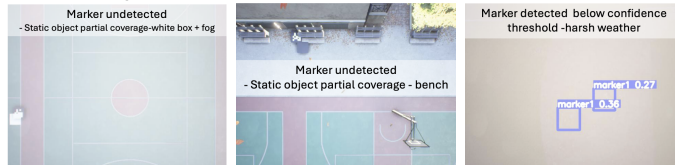
3) *Type III*: The third violation, UAV collision with static objects, occurs when the UAV, detecting a marker and initiating landing, fails to evade nearby branches, resulting in a collision (Figure 8c). Rviz visualization (Figure 8d) shows minor discrepancies between planned and actual trajectories, indicating that slight deviations can lead to collisions near markers surrounded by branches.

4) *Type IV*: The fourth violation, involving UAV collisions with moving objects, is illustrated in Figure 8e, where a UAV does not alter its descent path in response to a dog approaching the marker, resulting in a collision. Analysis indicates that moving ground-level objects, such as the dog, minimally affect the depth data visualized by Rviz, pointing to a low detection sensitivity for objects at low heights. This issue likely stems from the ego-planner’s limited capability in processing depth information, a theory supported by real-world experiments.

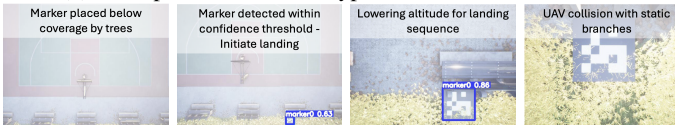
5) *Type V*: The fifth violation, a system-level crash, occurs when a dynamic object moves under a landing UAV, causing the planner to halt landing due to “the terminal point of



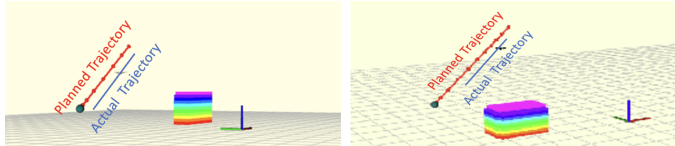
(a) Examples of Violation Type I: UAV lands on a false positive location due to wrong detection



(b) Examples of Violation Type II: No marker is detected



(c) Examples of Violation Type III: Static Object Collision



(d) Examples of trajectory difference visualized from Rviz



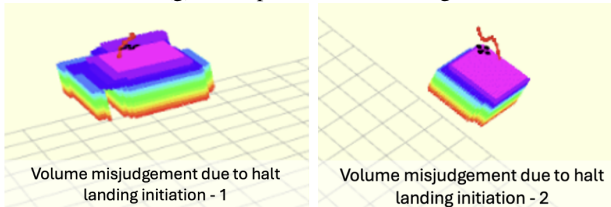
(e) Examples of Violation Type IV: Dynamic Object Collision



(f) Examples of Violation Type V: Planner Crash

```
WARN [1710207304, 49982600, 1710207304, 92816381]: [WARN] current point of the current trajectory is in obstacle, skip this planning
WARN [1710207304, 51544600, 1710207304, 94817473]: [WARN] current point of the current trajectory is in obstacle, skip this planning
WARN [1710207304, 52705600, 1710207304, 96817532]: [WARN] current point of the current trajectory is in obstacle, skip this planning
WARN [1710207304, 53866600, 1710207304, 98818118]: [WARN] current point of the current trajectory is in obstacle, skip this planning
WARN [1710207304, 55027600, 1710207304, 100818641]: [WARN] current point of the current trajectory is in obstacle, skip this planning
```

(g) Example of crash message



(h) Examples of the UAV stack in obstacle visualized from Rviz

Fig. 8: Examples of violations from simulation

TABLE III: Quantitative result of violation case generating efficiency and diversity for different methods, best is marked in bold.

Method	Metric	Court	Lawn
GARL	Landing violation %	20.60%	17.11%
	Top-10	42	76
	Parameter distance	0.19	0.19
	3D trajectory coverage%	11.24%	11.94%
Multi-Obj GA	Time Consumption (hours)	12	12
	Landing violation %	14.25%	9.23%
	Top-10	73	113
	Parameter distance	0.16	0.16
Random	3D trajectory coverage	4.92%	8.43%
	Time Consumption (hours)	11	11
	Landing violation %	9.37%	8.52%
	Top-10	205	112
Offline RL Fuzzer	Parameter distance	0.13	0.13
	3D trajectory coverage	3.51%	4.92%
	Time Consumption (hours)	11	11
	Landing violation %	2.25%	2.13%
Online RL	Top-10	cannot find	cannot find
	Parameter distance	0.12	0.12
	3D trajectory coverage	1.41%	3.51%
	Time Consumption (hours)	11	11
Surrogate trained RL with random scenario	Landing violation %	12.75%	5.94%
	Top-10	104	141
	Parameter distance	0.13	0.13
	3D trajectory coverage	4.92%	7.03%
	Time Consumption (hours)	11	11
	Landing violation %	14.19%	13.53%
	Top-10	67	108
	Parameter distance	0.13	0.13
	3D trajectory coverage	8.43%	8.43%
	Time Consumption (hours)	12	12

current trajectory is in obstacle” error (Figures 8f, 8g). Analysis indicates that proximity to moving obstacles can lead to volume misjudgment by the ego-planner, risking a crash (Figure 8h), a finding confirmed by real-world experiments. The detailed distribution of violation types across three landing systems in two maps can be found in the supplementary material.

B. Comparison to Baselines (RQ2)

As shown in Table III, GARL achieved the best performance on both maps across all metrics. On the Court map, GARL found 20.60% more violations, up to 18.35% better than SOTA methods in 400 runs. It excelled in diversity, with the highest Parameter distance (0.19) and 3D-Trajectory coverage (0.16%). GARL also required only 42 test cases to reveal the **Top-10** bugs. Similar results were observed for the Lawn map. Moreover, GARL has a similar time consumption compared to other baselines. Since all testing methods require running the test in the simulation while the RL agent runs side-by-side with the Airsim simulator on the same machine and calls the Airsim API, the running time overhead is mainly due to collision avoidance planning and the longer trajectory of flight caused by the complex interplay with the trajectory of dynamic objects. The overall time difference between methods is not significant. For example, running 400 test budgets for GARL and surrogate-trained RL with random scenarios takes around 12 hours on an RTX 3090 GPU, compared to 11 hours for other baselines. However, our method requires an additional 12 hours for training the RL agent in the surrogate environment, which is only needed once for all the maps. For the computational resources necessary for RL, we use a two-layer MLP, which requires just 2GB of GPU memory. We include a more detailed statistical analysis of all baselines in the supplementary material.

For *Multi-Objective GA*, performance on the *Lawn* map is only slightly better than the *Random* baseline. This is because GA often passes on configurations causing violations. Most violations in *Lawn* are due to collisions, which *Multi-Objective GA* struggles to detect. The *Surrogate trained RL with random scenario* baseline performs closely to GARL, highlighting the importance of online RL.

Both *Online RL* and *Offline RL Fuzzer* underperform. GA effectively reduces the learning space for RL training, with the GA-reduced RL agent converging in 800 episodes, compared to 4200 episodes for the full learning space. This highlights GA's advantage in facilitating efficient RL training. RL agents struggle to converge in complex real-world spaces without GA's targeted reduction. Detailed rewards figures are in the supplementary document.

GARL and the *Surrogate trained RL with random scenario* uniquely detected *Type IV* and *Type V* violations. However, without GA, the latter struggles in complex scenarios like the *Court* map. GA aids by identifying potential seeds for violation detection, simplifying RL's requirements, and highlighting promising candidates, especially in complex scenarios.

C. Real-World Reproduction (RQ3)

We validated the identified violation cases in simulations with real-world tests. We reproduced *Type I* and *Type II* violations on a lakeside lawn under sunny conditions, a constrained physical environment. The test used a $0.75m \times 0.75m$ marker and a UAV flying at a height of $5m$, scaled to 50% of the simulation setting. Figure 9a shows a *Type II* false negative detection where the marker is initially identified but becomes undetectable when partially obscured by a branch. Figure 9b shows a *Type I* false positive detection where a person wearing a black hoodie is detected as the ArUco marker.

For *Type III* violations, we did not reproduce the scenario in the real world due to safety concerns. Validating this type would require allowing the UAV to execute its planned trajectory, which was deemed infeasible. The real-world performance of a UAV with only GPS input typically has a position estimate accurate within 1 meter [22]. However, GPS signal loss can cause larger deviations [46]. The identified violation underscores the need for more robust UAV landing solutions and demonstrates our framework's capability to help developers identify subtle issues earlier in the development lifecycle.

For *Type IV* violations, as shown in Figure 9c, a real-world scenario was observed where a ball moving across the depth camera's field of view did not alter the captured depth information, potentially leading to a collision during the UAV's landing phase. This issue aligns with our simulation experiment, where near-ground objects like dogs are not detected as obstacles and cause collisions, as shown in Figure 8e.

For *Type V* violations, a quick movement of an object closely beneath the UAV can trigger a crash in the planner. In the real-world test shown in Figure 9d, the planner initially captures depth information accurately. However, when a chair is rapidly moved underneath the UAV, it is perceived as an obstacle,

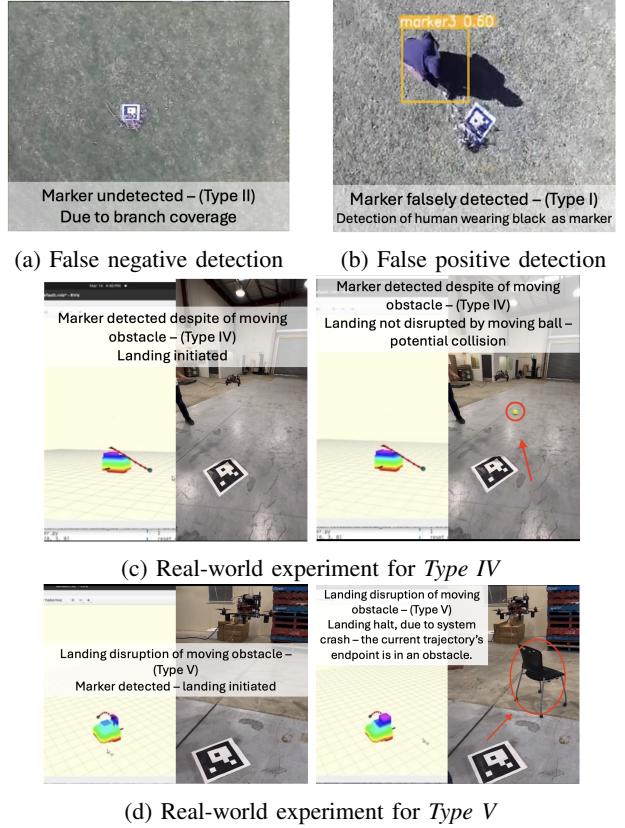


Fig. 9: Example of real-world violations reproduction

raising the error “the terminal point of current trajectory is in obstacle”, underscoring the issue’s relevance in real scenarios.

VI. THREATS TO VALIDITY

Construct Validity: The construct validity is challenged by adapting landing systems and baseline methods for comparison. We developed three auto-landing systems: *OpenCV-MLS*, *TPHYolo-MLS*, and *MM-MLS*. Three marker-based landing systems were selected to represent different capability levels and demonstrate iterative evolution through our testing approach. *OpenCV-MLS*, the only open-source baseline implementation [24] used by our industry partner, initially struggled with detecting small markers. To improve accuracy and robustness, we integrated the *TPHYolo* detector, known for detecting small objects in UAV images, creating *TPHYolo-MLS*. The most robust system, *MM-MLS*, enhances *TPHYolo-MLS* by adding the *Ego-planner*, a state-of-the-art path planner for real-time, collision-free navigation, similar to industrial autonomous driving systems like *Apollo* and *Autoware*. This selection illustrates iterative improvements enabled by our testing methodology, with each system representing a progression in functionality, allowing us to evaluate how effectively GARL identifies issues and drives enhancements toward a more robust and reliable marker-based landing system.

Due to limited research on testing marker-based landing systems, direct baseline methods are challenging to find. We adopted state-of-the-art search-based [59], fuzzer [9], and

online [40] test generation methods from the software testing community, aligning their fitness or reward functions with ours. Although we found a method called Adaptive Stress Testing with backward training [32], we did not compare it because RL with a full learning space fails to converge even in a simplified surrogate environment, making it impractical to obtain expert trajectories for backward training. The training curves can be found in the supplementary material.

Another construct validity issue arises from GPS errors. In the simulation environment, we did not account for GPS errors because AirSim provides ground truth GPS data and lacks interfaces for modifying it. However, when setting up markers, we randomly positioned the center point within a 7.5-meter radius of the marker's GPS coordinate. The vision-based landing system is designed to handle inaccurate GPS landing locations. In real-world experiments, we considered GPS as a potential factor for Type III violations (collisions with static objects). To reproduce other violation cases, we tested the system in a stable GPS environment. Additionally, during flights, the ArduPilot controllers use the Extended Kalman Filter (EKF) to manage potential GPS errors [5].

External Validity: The primary external validity concern is the generalizability of our method. To tackle this, we tested our search method across various landing systems, including *OpenCV-MLS*, *TPHYolo-MLS*, and *MM-MLS*, and on maps representing real-world deployment sites of our industry partners. Our method successfully identified diverse violation cases across these landing systems and maps.

Internal Validity: A potential threat to internal validity is the fidelity of the simulation environment. To address this concern, we chose maps relevant to real-world applications. The marker-based landing system we tested is designed for delivery purposes. Our industry research collaborators target grassy lawns and concrete hospital courts with additional markings and ground obstacles. The lawn map represents rural farms for logistics delivery, while the basketball map represents hospital and industrial zones for urgent components and medical supplies delivery. For each deployment map, we incorporated dynamic objects found in the actual deployment sites into AirSim. We ensured our maps closely resembled real deployment environments. Positive outcomes from our real-world tests further alleviate this validity concern.

Another potential threat is real-world reproduction. To replicate the simulation results, we adjusted controllable environmental factors and considered uncontrollable ones like dust, fog, and snow. Adjustable factors included marker locations, nearby objects, time of day for lighting changes, and a regulated wind speed of 3 m/s for lakeside tests. For type I (wrongly recognizing markers) and type II (missing true markers) violations, we varied marker locations, placed objects near markers, and conducted tests at different times of the day. We configured the simulation's camera parameters based on physical camera specifications and aligned the UAVs' flight control parameters to replicate the tested flight patterns. Our simulation platform and testing methods generated detailed logs for fault analysis, as shown in the RQ1 results (P8). We

successfully reproduced these violations in real-world settings based on identified root causes. However, we faced limitations not present in the simulation, such as minor lens stains, blurry images, excessive glare, and poor network connections affecting detection models. These issues could trigger violations in real-world testing. We plan to conduct extensive field testing with industry partners in diverse environments to gather feedback. This feedback will help build a more high-fidelity co-simulation or hardware-in-the-loop simulation platform with Simulink.

VII. DISCUSSION

Our approach effectively detects issues in path planning, which is crucial for UAV safe landing, monitoring, surveying, and other autonomous systems, including vehicles. This method can be applied early in the software development life cycle, during the prototype and design stages, to detect bugs and guide design choices for machine learning models and system architecture. Early detection helps avoid costly fixes post-deployment. Using our simulation platform, we detected bugs and improved landing solutions, resulting in three generations of auto-landing systems with different machine learning models and architectures. Our method also aids in business operation risk assessment to identify potential risks and determine safe deployment areas, and detect early bugs in other critical components, such as the perception module.

Using RL for online testing is challenging due to difficulties in training agents to converge in complex action spaces. GARL allows practitioners to conduct a one-time surrogate training period of approximately 12 hours for our landing system action spaces, after which the trained agent can be applied across various maps and deployment environments in simulation. This method is effective in detecting subtle and complex issues, particularly in path planning, a crucial component in many autonomous systems. Early detection during the prototype and design stages is cost-effective and can significantly influence design decisions. For example, we successfully used this approach to modify key perception models, path planning, and architecture in three landing systems.

VIII. CONCLUSION

This paper introduces a method for generating diverse violation cases in marker-based UAV landing systems. Our approach integrates GA to reduce the RL search space and a low-fidelity proxy to improve RL convergence. Experiments show that GARL detects 18.35% more violations with 58% greater diversity than existing methods, uncovering previously undetected violation types validated in real-world tests. These findings highlight GARL's efficacy in early error detection, enhancing safety and reducing costs. Future work includes extending the RL algorithm to multi-agent RL for collaborative behaviors, broadening test scenarios, and applying GARL to learning-enabled autonomous systems like vehicles and humanoid robots.

ACKNOWLEDGEMENT

This work is supported by Australia Research Council grants LP210100337, LP190100676, and DP210102447.

REFERENCES

- [1] Abdessalem, R.B., Panichella, A., Nejati, S., Briand, L.C., Stifter, T.: Testing autonomous cars for feature interaction failures using many-objective search. In: Proceedings of the 33rd ACM/IEEE International Conference on Automated Software Engineering. pp. 143–154 (2018)
- [2] Administration, F.A.: (2022), <https://www.faa.gov/uas>
- [3] Aero, S.: Kite. <https://swoop.aero/technology/kite/> (2022), retrieved June 14, 2024
- [4] ApolloAuto: Apollo. <https://github.com/ApolloAuto/apollo> (2024)
- [5] ArduPilot: Apm navigation: Extended kalman filter overview. <https://shorturl.at/mmDOR> (2024), retrieved June 14, 2024
- [6] Ardupilot: Ardupilot (2024), <https://github.com/ArduPilot/ardupilot>.
- [7] Baca, T., Stepan, P., Spurny, V., et al.: Autonomous landing on a moving vehicle with an unmanned aerial vehicle. *Journal of Field Robotics* **36**(5), 874–891 (2019)
- [8] Ben Abdessalem, R., Nejati, S., Briand, L.C., Stifter, T.: Testing advanced driver assistance systems using multi-objective search and neural networks. In: Proceedings of the 31st IEEE/ACM international conference on automated software engineering. pp. 63–74 (2016)
- [9] Böttlinger, K., Godefroid, P., Singh, R.: Deep reinforcement fuzzing. In: IEEE Security and Privacy Workshops (SPW). pp. 116–122. IEEE (2018)
- [10] Bradski, G.: The OpenCV Library. Dr. Dobb's Journal of Software Tools (2000)
- [11] Brunner, G., Szebedy, B., Tanner, S., Wattenhofer, R.: The urban last mile problem: Autonomous drone delivery to your balcony. In: 2019 international conference on unmanned aircraft systems (icuas). pp. 1005–1012. IEEE (2019)
- [12] CASA: Drone rules (2022), ‘<https://www.casa.gov.au/knowyourdrone/drone-rules>
- [13] Chen, L., Yuan, X., Xiao, Y., Zhang, Y.: Robust autonomous landing of uav in non-cooperative environments based on dynamic time camera-lidar fusion (2020)
- [14] Deb, K., Agrawal, S., Pratap, A., Meyarivan, T.: A fast elitist non-dominated sorting genetic algorithm for multi-objective optimization: Nsga-ii. In: Parallel Problem Solving from Nature PPSN VI: 6th International Conference Paris, France, September 18–20, 2000 Proceedings 6. pp. 849–858. Springer (2000)
- [15] Deng, Y., Zheng, X., Zhang, M., Lou, G., Zhang, T.: Scenario-based test reduction and prioritization for multi-module autonomous driving systems. In: Proceedings of the 30th ACM Joint European Software Engineering Conference and Symposium on the Foundations of Software Engineering. pp. 82–93 (2022)
- [16] DJI Enterprise: DJI Dock2. <https://enterprise.dji.com/dock-2> (nd), retrieved June 14, 2024
- [17] Dronehub: Dronehub. <https://dronehub.ai/> (nd), retrieved June 14, 2024
- [18] Ebadi, H., Moghadam, M.H., et al.: Efficient and effective generation of test cases for pedestrian detection-search-based software testing of baidu apollo in syl. In: 2021 IEEE International Conference on Artificial Intelligence Testing (AITest). pp. 103–110. IEEE (2021)
- [19] Epic Games: Unreal engine, <https://www.unrealengine.com>, accessed 2019-04-25
- [20] Esnaashari, M., Damia, A.H.: Automation of software test data generation using genetic algorithm and reinforcement learning. *Expert Systems with Applications* **183**, 115446 (2021)
- [21] Feng, S., Sun, H., Yan, X., et al.: Dense reinforcement learning for safety validation of autonomous vehicles. *Nature* **615**(7953) (2023)
- [22] Fornasier, A., Ge, Y., et al.: An equivariant approach to robust state estimation for the ardupilot autopilot system
- [23] Garrido-Jurado, S., Muñoz-Salinas, R., et al.: Automatic generation and detection of highly reliable fiducial markers under occlusion. *Pattern Recognition* **47**(6), 2280–2292 (2014)
- [24] Goodrobots: Vision landing. https://github.com/goodrobots/vision_landing (nd), retrieved June 14, 2024
- [25] Haq, F.U., Shin, D., Briand, L.: Many-objective reinforcement learning for online testing of dnn-enabled systems. *arXiv preprint arXiv:2210.15432* (2022)
- [26] Hu, Z., Guo, S., Zhong, Z., Li, K.: Coverage-based scene fuzzing for virtual autonomous driving testing. *arXiv preprint arXiv:2106.00873* (2021)
- [27] Huai, Y., Almanee, S., Chen, Y., Wu, X., Chen, Q.A., Garcia, J.: sceno rita: Generating diverse, fully-mutable, test scenarios for autonomous vehicle planning. *IEEE Transactions on Software Engineering* (2023)
- [28] Kam, H.R., Lee, S.H., et al.: Rviz: a toolkit for real domain data visualization. *Telecommunication Systems* **60**, 337–345 (2015)
- [29] Khadka, S., Turner, K.: Evolution-guided policy gradient in reinforcement learning. *Advances in Neural Information Processing Systems* **31** (2018)
- [30] Khazetdinov, A., Zakiev, A., Tsoy, T., Svinin, M., Magid, E.: Embedded aruco: a novel approach for high precision uav landing. In: 2021 International Siberian Conference on Control and Communications (SIBCON). pp. 1–6. IEEE (2021)
- [31] Koren, M., Alsaif, S., Lee, R., Kochenderfer, M.J.: Adaptive stress testing for autonomous vehicles. In: 2018 IEEE Intelligent Vehicles Symposium. IEEE (2018)
- [32] Koren, M., Nassar, A., Kochenderfer, M.J.: Finding failures in high-fidelity simulation using adaptive stress testing and the backward algorithm. In: 2021 IEEE/RSJ International Conference on Intelligent Robots and Systems (IROS). IEEE (2021)
- [33] Lai, K.T., Chung, Y.T., et al.: Ai wings: an aiot drone system for commanding ardupilot uavs. *IEEE Systems Journal* (2022)
- [34] Lee, B., Saj, V., Kalathil, D., Benedict, M.: Intelligent vision-based autonomous ship landing of vtol uavs. *Journal of the American Helicopter Society* **68**(2) (2023)
- [35] Lehman, J., Stanley, K.O.: Abandoning objectives: Evolution through the search for novelty alone. *Evolutionary computation* **19**(2), 189–223 (2011)
- [36] Lehman, J., Stanley, K.O., et al.: Exploiting open-endedness to solve problems through the search for novelty. In: ALIFE. pp. 329–336 (2008)
- [37] Li, G., Li, Y., Jha, S., et al.: Av-fuzzer: Finding safety violations in autonomous driving systems. In: 2020 IEEE 31st international symposium on software reliability engineering (ISSRE)
- [38] Lin, S., Jin, L., Chen, Z.: Real-time monocular vision system for uav autonomous landing in outdoor low-illumination environments. *Sensors* **21**(18), 6226 (2021)
- [39] Lou, G., Deng, Y., et al.: Testing of autonomous driving systems: where are we and where should we go? In: Proceedings of the 30th ACM Joint European Software Engineering Conference and Symposium on the Foundations of Software Engineering. pp. 31–43 (2022)
- [40] Lu, C., Shi, Y., et al.: Learning configurations of operating environment of autonomous vehicles to maximize their collisions. *IEEE Transactions on Software Engineering* **49**(1), 384–402 (2022)
- [41] Lu, Y., Shao, K., Sun, W., Sun, M.: Rgchaser: A rl-guided fuzz and mutation testing framework for deep learning systems. In: 2022 9th International Conference on Dependable Systems and Their Applications (DSA). pp. 12–23. IEEE (2022)
- [42] Luo, Y., Zhang, X.Y., et al.: Targeting requirements violations of autonomous driving systems by dynamic evolutionary search. In: 2021 36th IEEE/ACM International Conference on Automated Software Engineering (ASE). pp. 279–291. IEEE (2021)
- [43] Marchesini, E., Farinelli, A.: Genetic deep reinforcement learning for mapless navigation. In: Proceedings of the 19th International Conference on Autonomous Agents and MultiAgent Systems. pp. 1919–1921 (2020)
- [44] Marcu, A., Costea, D., Licaret, V., Pirvu, M., Slusanschi, E., Leordeanu, M.: Safeuav: Learning to estimate depth and safe landing areas for uavs from synthetic data. In: Proceedings of the European Conference on Computer Vision (ECCV) Workshops. pp. 0–0 (2018)
- [45] Mittal, M., Mohan, R., Burgard, W., Valada, A.: Vision-based autonomous uav navigation and landing for urban search and rescue. In: The International Symposium of Robotics Research. pp. 575–592. Springer (2019)
- [46] Pang, B., Ng, E.M., Low, K.H.: Uav trajectory estimation and deviation analysis for contingency management in urban environments. In: AIAA Aviation 2020 Forum. p. 2919 (2020)
- [47] Panichella, A., Kifetew, F.M., Tonella, P.: Reformulating branch coverage as a many-objective optimization problem. In: 2015 IEEE 8th international conference on software testing, verification and validation (ICST). pp. 1–10. IEEE (2015)
- [48] Percepto: Drone-in-a-box. <https://percepto.co/drone-in-a-box/> (nd), retrieved June 14, 2024
- [49] Prathiba, S.B., Raja, G., Dev, K., Kumar, N., Guizani, M.: A hybrid deep reinforcement learning for autonomous vehicles smart-platooning. *IEEE Transactions on Vehicular Technology* **70**(12), 13340–13350 (2021)
- [50] Schmidt, T., Pretschner, A.: Stellaauv: A tool for testing the safe behavior of uavs with scenario-based testing (tools and artifact track). In: 2022 IEEE 33rd International Symposium on Software Reliability Engineering (ISSRE) (2022)

- [51] Shah, S., Dey, D., Lovett, C., Kapoor, A.: Airsim: High-fidelity visual and physical simulation for autonomous vehicles. In: Field and Service Robotics (2017), <https://arxiv.org/abs/1705.05065>
- [52] Shakhatreh, H., Sawalmeh, A.H., Al-Fuqaha, A., Dou, Z., Almaita, E., Khalil, I., Othman, N.S., Khreichah, A., Guizani, M.: Unmanned aerial vehicles (uavs): A survey on civil applications and key research challenges. *Ieee Access* **7**, 48572–48634 (2019)
- [53] Shimada, T., Nishikawa, H., Kong, X., Tomiyama, H.: Pix2pix-based monocular depth estimation for drones with optical flow on airsim. *Sensors* **22**(6), 2097 (2022)
- [54] Skyy: Medlife and skyy network partner to introduce romania's first medical delivery network. <https://shorturl.at/QgPsy> (nd), retrieved June 14, 2024
- [55] Skyy: Windjammer landing resort. <https://shorturl.at/w9UsB> (nd), retrieved June 14, 2024
- [56] Song, Y., Steinweg, M., Kaufmann, E., Scaramuzza, D.: Autonomous drone racing with deep reinforcement learning. In: 2021 IEEE/RSJ IROS. pp. 1205–1212. IEEE (2021)
- [57] Stafylopatis, A., Blekas, K.: Autonomous vehicle navigation using evolutionary reinforcement learning. *European Journal of Operational Research* **108**(2), 306–318 (1998)
- [58] Sutton, R.S., Barto, A.G.: Reinforcement learning: An introduction. MIT press (2018)
- [59] Tian, H., Jiang, Y., et al.: Mosat: finding safety violations of autonomous driving systems using multi-objective genetic algorithm. In: ESEC/FSE 2022. pp. 94–106 (2022)
- [60] Van Hasselt, H., Guez, A., Silver, D.: Deep reinforcement learning with double q-learning. In: Proceedings of the AAAI conference on artificial intelligence. vol. 30 (2016)
- [61] Vaswani, A., Shazeer, N., et al.: Attention is all you need. *Advances in neural information processing systems* **30** (2017)
- [62] Vetrella, A.R., Fasano, G., Renga, A., Accardo, D.: Cooperative uav navigation based on distributed multi-antenna gnss, vision, and mems sensors. In: 2015 International Conference on Unmanned Aircraft Systems (ICUAS). IEEE (2015)
- [63] Vincent, J.: Food delivery drone lands on power lines resulting in power outage for thousands. ABC News (2022-09-30), <https://shorturl.at/KqQju>
- [64] Wegener, J., Bühler, O.: Evaluation of different fitness functions for the evolutionary testing of an autonomous parking system. In: Genetic and Evolutionary Computation—GECCO 2004: Genetic and Evolutionary Computation Conference, Seattle, WA, USA, June 26-30, 2004. Proceedings, Part II. pp. 1400–1412. Springer Berlin Heidelberg (2004)
- [65] Wingcopter: Technical details: Wingcopter 178 heavy lift a delivery variant. <https://shorturl.at/OE5QD> (nd), retrieved June 14, 2024
- [66] Xu, S., Bi, W., Zhang, A., Wang, Y.: A deep reinforcement learning approach incorporating genetic algorithm for missile path planning. *International Journal of Machine Learning and Cybernetics* **15**(5), 1795–1814 (2024)
- [67] Zheng, Y., Xie, X., et al.: Wuji: Automatic online combat game testing using evolutionary deep reinforcement learning. In: 2019 34th IEEE/ACM International Conference on Automated Software Engineering (ASE). pp. 772–784. IEEE (2019)
- [68] Zhong, Z., Kaiser, G., Ray, B.: Neural network guided evolutionary fuzzing for finding traffic violations of autonomous vehicles. *IEEE Transactions on Software Engineering* (2022)
- [69] Zhou, X., Wang, Z., Ye, H., Xu, C., Gao, F.: Ego-planner: An esdf-free gradient-based local planner for quadrotors. *IEEE Robotics and Automation Letters* **6**(2), 478–485 (2020)
- [70] Zhu, X., Lyu, S., Wang, X., Zhao, Q.: Tph-yolov5: Improved yolov5 based on transformer prediction head for object detection on drone-captured scenarios. In: Proceedings of the IEEE/CVF international conference on computer vision. pp. 2778–2788 (2021)